

# Riveted Panel Surface Measurement Using Photogrammetry

W. D. Merrick, V. B. Lobb,  
F. L. Lansing and F. W. Stoller  
Ground Antenna and Facilities Engineering Section

*Two riveted antenna panels on rings number 3 and 9 were removed from the 34m antenna at DSS-15, fixed in the leveled position and the surface was photographed indoors. The results from this pilot photogrammetric demonstration and diagnostics of panel surface contours, are presented. The photogrammetric network for each panel incorporated eight photographs, two from each of four camera stations and observed over 200 targets. The accuracy ( $1\sigma$ ) of the XYZ coordinates for the error ellipsoids was  $\pm 0.013$  mm (0.0005 inch). This level of precision relative to the object size corresponds roughly to 1 part in 250,000 which is superior to conventional dial sweep-arm template techniques by at least a factor of 4.*

## I. Introduction

During the construction of the NASA-JPL 34m High Efficiency (HE) antennas at DSS-15 and DSS-45, two identical sets of surface panel inspection jigs using sweep-arm templates were provided. One set was for use during panel fabrication and the other set for field inspection at the construction site prior to panel installation on the antenna. Single panel samples from each of the nine antenna rings differed in their measured surface accuracies when inter-compared in both sets of sweep-arm jigs.

Photogrammetric measurements (PGM) as a pilot demonstration on two sample panels were performed to resolve the above jig measurement disparities. By use of a more precise metrology technique such as PGM the demonstration provided also the means for validation of the cost, accuracy, speed of measurement, and the work-time spans required for future projects.

Geodetic Services Inc. (GSI), under contract with the Jet Propulsion Laboratory, performed the PGM field measurements, and data processing. The contractor, GSI, was selected by means of a wide survey of U.S. and Canadian vendors. GSI has introduced and practiced many new technologies in close-range photogrammetry over the past two decades. These include: the bundle method of processing photogrammetric triangulation, calibration procedures, instrumentation upgrades and field practices. As a result, the contractor has developed the best available precision and versatile specialized photogrammetric equipment, (Refs. 1–5).

This article describes the measurement procedure, the hardware and the software technologies.

## II. Test Procedure

Similar to installation upon the operational antenna structure, the two shaped-contour panels were tested while sup-

ported upon the adjusting 4-6 corner screws as shown in Figs. 1-4. The small panel (from antenna ring No. 3) has the dimensions of 2.0 X 2.7 m (6.5 X 7 ft) and the larger panel (from outer ring No. 9) has the dimensions of 2.1 X 2.7 m (7 X 9 ft). Small stick-on photogrammetric retrotargets were installed on the faces of the two panels at locations close to those previously measured by the jigs. The positions of reference targets were measured to provide a tie to global antenna coordinates.

Four points on each panel were leveled and the targets near the other adjustment screws were brought to the proper design heights. Then, the Z coordinates (vertical elevations) of all targets were observed with the same precision level (a calibrated Swiss-made Wild N3 instrument). The test conditions were indoors, in shaded and air conditioned space. The panels were supported by steel fixtures that rested upon a thick concrete slab well isolated from room vibrations.

The four key photogrammetry elements needed are: (1) the camera, (2) the film digitizer (comparator), (3) the computer, and (4) the software. The procedure may be summarized as follows: A two-person crew, used a special photogrammetric camera to take pictures of the several hundred small, self-adhesive 1-cm diameter retrotargets installed upon each panel. The completion of these photos required only a few hours at the demonstration site. Note that actual photogrammetric accuracy improves in proportion to the square root of the number of photos.

The coordinates of each target image were "read" automatically on a special film digitizer at the contractor's facility in Melbourne, Florida. After reading the film data, the (X, Y, Z) coordinates of each target are computed. The rays from all camera stations converging at a given target determine an individual error ellipsoid for that target. Using least squares techniques, the semi-axes of the ellipsoids are obtained for each target. The PGM technique proved advantageous as a high accuracy, low cost with short measurement time technique (less than one hour per camera network). The demonstration employed the main eight ingredients needed for the highest accuracy in photogrammetry which are listed below:

- (1) The use of the bundle method in triangulation with self-calibration of all elements of each independent photogrammetric network.
- (2) The use of highly convergent photography for maximum geometric strength.
- (3) The use of a long focal length, large format camera.
- (4) The use of a large number of exposures in simultaneous bundle data reduction.

- (5) The use of roll film and vacuum registry against a stable camera platen equipped with integral reseau projectors.
- (6) The use of analytical compensation for the variation of image distortion with object distance (e.g., diffraction).
- (7) The use of a computer based Simulator for planning of optimum PGM networks and operational fieldwork.
- (8) The calibration of the lens' radial, decentering and other distortions, as well as the camera cone and platen imperfections.

### III. Test Equipment

The single GSI CRC-1 camera with a 240 mm (9.45 in.) focal length lens and cone was moved between the camera stations. The selected film was Kodak Tech Pan rated at approximately 200 ASA. By utilization of the proper developer, a single step grey scale was attained which suppressed the extraneous details of the object being measured. Even if the object had been in bright sunlight, the full target details would have been retained. A strobe flash located proximate to the camera lens, was used to 'turn on' the adhesive-backed retrotargets (fabricated from 3M type 7610 beaded material).

Convergent imaging geometry was employed. Before conducting the field tests, a computer based Simulator was used to optimize and identify the positions of the desired camera stations as in Fig. 5, to enhance the geometric strength and reliability of the triangulation. Photography of the object from movable stations was simulated to provide the maximum possible convergence angles; those which improve the accuracy in the Z direction so that it approaches the accuracy of the X, Y coordinates.

The camera was located upon an air-actuated vertical service lift at approximately 3.8 m (12.5 ft) above the panel corners. With the tripod, camera and operator in place upon the platform, the outriggers were raised or lowered and the service lift was moved manually by two men.

Absolute scale was established by means of known distances between targets attached to a thermally stable surveying tape positioned across the face of each panel as shown in Fig. 2. The film was developed on site under controlled processing temperature.

The images of the targets were automatically read and the digitized coordinates recorded on the GSI AutoSet-1 mono-comparator located at the contractor's facility. Since the comparator is mounted upon a thick granite slab, it is the

only non-mobile (but relocatable) element in the PGM system. This fully automated film reader has a resolution of under 0.1 micron (4 micro inch) and is accurate to about 0.4 micron (16 micro inch) in each of the two coordinate axes. The Simulator results in the images of the center dots of the targets being about 75 microns in diameter. The area of each dot image is digitized into 400 to 750 pixels. The statistical centroid is computed, and the image is automatically re-centered by the comparator before the coordinates are recorded, thereby eliminating the reading bias error associated with a human operator.

Multiple camera roll angles were used to improve the accuracy of each network. When properly handled in photogrammetric computations, rotating the camera about the axis of the lens serves to cancel out all lens, lens cone and camera error except platen non-flatness (which is measured by other techniques and is fully compensated for in the reduction of the data).

The deleterious effects of distortion of the film emulsion and film base, are eliminated by reading, within the camera, the position of 25 "target-like" calibration images that are projected through the film backing onto every film frame by patented reseau projectors (mounted in the precision film platen made from temperature-stable material). The reseau images are located so that the target images are never more than 35 mm from the nearest reseau image. Four additional calibration images are projected onto the front face of each film frame from projectors located near the camera lens.

The outer ring of each of the retrotargets validates that the film was in contact (actuated by vacuum) with the special stable camera platen at the time of film exposure. If the outer ring of the image of the target shows as a crescent instead of a full circle, the suspect image/point is read and recorded with a weight of zero. At a later time, by measuring the dimensions of the ring image, an operator completes the computations required to recover the precise data for the center of that imperfect image.

The comparator-measured X, Y coordinates were then processed through a series of computer programs which provide rigorous simultaneous, least squares spatial triangulation and bundle adjustment of all measured data. "Bundling" denotes the reduction of large matrices into a plethora of smaller sparse ones that may be handled by simple known methods.

The self-calibration processes described above act to minimize the volumes of the error ellipsoid(s) which result from the non-intersection of the convergent rays that determine the Cartesian coordinates of each and every camera station and

target/point. The three values for the semi-axes of each error ellipsoid are computed. Ultimately, the X, Y, Z space coordinates for each target/point (and each camera lens station) are determined. The accuracy of the coordinates is independent of the nature of the photographed object.

#### IV. Test Time Span

For future planning purposes, it was essential to establish work-time relationships for estimating PGM measurement time spans, workhours and operational costs. Table 1 delineates the activities that occurred during the test period.

Experience shows that repetition of a given photogrammetric task usually requires less time to complete than the prototype operation. For example, our "first time" film reading (23 cm X 23 cm format) took 4 frames per hour. A second time iteration with the same crew would take 8 frames per 1.5 hour. The triangulation and bundling software takes about 0.5 hour to complete in either case. Our "first time" task required field photography and film development by two men working 10 hours on site, plus travel time.

In summary, the PGM demonstration took 6 hours to measure two panels, 5 days to complete the whole task, and 1 minute/frame to film the last network (includes camera movement).

#### V. System Simulation

Figure 5 illustrates the relative camera-panel locations for simulation and Figs. 6-9 give the Simulator output for optimum PGM accuracy. Note that the targets are shown covering the full area of the panels, but the operator has opted for fewer targets for easier screen perusal. The Simulator data appear at the left hand side of Figs. 6-9; and it further generates expected standard deviation (1-sigma) accuracy, image diameters, depth of field, etc. The accuracy that would be expected from networks where one film frame was exposed at each of four camera stations is given in Table 2 as 0.033 mm (0.0013 inch) for the Z-axis.

The initial formulations of the Simulator were conservative. When implemented, the resultant field accuracy exceeded the requirements. References to Tables 2 and 3 shows that the ratio of the accuracy predicted by the Simulator to the delivered accuracy, was 0.033 mm/0.013 mm or 2.6/1. This improved ratio results because doubling the number of films exposed at each station increased the accuracy ratio by a factor of 1.41.

In Building G-84 at the Mars Deep Space Station, heavy equipment stored along the walls prevented the service lift

(and supported camera) from occupying the optimum camera stations as determined by the Simulator. Since this was also a "first time" demonstration, the crew exposed two photographs at each camera station with differing flash lamp intensities (100 Ws and 200 Ws). Two camera roll angles of 135 and 235 degrees were used also to cancel out potential error contributions from the camera.

The Z axis runs near the center (or lowest point) of each panel, perpendicular to the plane taken through three points (located near the corners of each panel). In Fig. 5 these corner reference points are labeled A, B, C. For the larger panel, the three points were targets number 101, 110 and 1701; and for the smaller panel these were number 101, 108 and 1301. For the larger panel, the Y-axis is parallel to the line joining points 101 and 110, and the X-axis runs parallel to the line joining points 110 and 1710. Hence, most of the points on each panel show negative Z coordinate values.

## VI. Leveling Screw Locations

Three targets (A, B, C) out of four in Fig. 10 were chosen adjacent to the panel-antenna backup truss adjustment leveling screws. In measuring points on the panel and in adjusting/leveling the antenna panels, the crew used a precision level with 10 seconds of arc per 2 mm dial bubble, prior to PGM. (More modern optical instruments incorporate an optical pendulum that automatically levels the sighting axis of the instrument). In an air-conditioned space, the Wild N3 instrument was sighted upon a vertical invar leveling rod placed in physical contact with the targets. The rounded end of the rod rested upon the top surface of the black overlay of the target.

Tables 4 and 5 show the Z departures from the reference plane (taken through three corner targets of the panels). Note from Table 5 that the fourth target D (No. 1710) lies 0.0078 inch (0.198 mm) above the reference plane formed by targets A, B, and C. Similarly, from Table 4 on the small panel No. 3, the fourth target D (No. 1308) adjacent to the fourth leveling screw was -0.0024 inch (0.061 mm) from the reference plane (formed by targets A, B and C).

Suppose that the reference plane for a panel had been relocated, to minimize the coplanar errors of four corner points (instead of three points on each panel), then, the Z coordinate offsets of the larger panel No. 9 would appear to be within  $\pm 0.0020$  inch (0.050 mm) at each corner; the Z-numbers changed but the panel did not. The above values suggest that the measuring accuracy resulting from the use of the Wild N3 level and the invar rod approaches  $\pm 0.002$  inch (0.050 mm) at short distances.

## VII. Test Results

The Simulator computed the predicted accuracy prior to the field work as in Table 2. The actual PGM results for all targets and camera stations are given in Table 3. The accuracy ( $1\sigma$ ) of all coordinates of both panels was better than 0.013 mm (0.0005 in.). This corresponds to a precision ratio relative to the object diameter between 1/230,000 to 1/270,000. Beginning at a minimum number of four camera stations, the accuracy of PGM self-calibrated triangulation improves directly as the square root of the number of rays (or lines) used to determine the location of each point/target, hence Table 6 is formed. Accuracies of 1/350,000 are possible, theoretically, with 16 rays per target.

Note that to demonstrate an accuracy better than 1 part in 350,000 would have required consideration of the thickness of each target (and in turn the additional thickness of the black overlay), the obliquity of the ray from the normal to the panel surface, and the separation of the nodal planes within the camera lens. Although the terms of these additional equations are straight-forward, there would have been additional computational expenses. Note also that theodolite accuracy peaks at a precision ratio of 1 part in 64,000 at best.

The two antenna panels are part of a contoured quasi-paraboloid (shaped) surface which usually requires 12 to 15 terms in a power series that characterize the main reflector surface. Appendix A is provided for reference by users who may wish to proceed with best-fitting of the data in order to determine RF path lengths, surface RMS, etc., for both parabolic or quasi-parabolic surfaces.

In addition, the riveted panel specifications were required to be checked with tooling accurate to  $\pm 0.076$  mm (0.003 in.). By using this pilot PGM demonstration, the two panels were measured to accuracies that were six times better.

## VIII. Future Work

Can the "not precisely levelled" panels coordinate data be transformed into the data that would have been recorded if the adjustment corner points (four to six points) had been perfectly positioned prior to the PGM test? If so, can an antenna panel be removed from the shipping crate when received at a site, "thrown" on the ground, photographed and the leveling done in a computer (instead of a sweep template jig) to detect possible damage during transport?

These thoughts could be used as the impetus for future work in software development to detect panel corner warping or panel stressing problems. Such capability should lead to a

better understanding of panel deflections and performance under loads, (Ref. 6) or the little traumas of shipping.

If adequate accuracy can be obtained in this process of converting photogrammetric panel data, the future might include such possibilities as:

- (1) Obviate the use/need for quality assurance (QA) inspection jigs and sweep templates.

- (2) Eliminate the expensive labor paid for the adjustment of the panels in the jigs.

- (3) Shorten scheduling spans.

- (4) Provide a measuring accuracy of better than 0.025 mm (0.001 inch) that is only 20 percent of the 0.13 mm (0.005 inch) high quality panel tolerance (rms) requirements planned for future antennas.

## References

1. Brown, D. C., *The Simultaneous Determination of the Orientation and Lens Distortion of a Photogrammetric Camera*, RCAMTP Data Reduction Technical Report No. 33, Patrick Air Force Base, Florida, 1956.
2. Brown, D. C., *Evolution, Application and Potential of the Bundle Method of Photogrammetric Triangulation*, International Society for Photogrammetry, Commission III, Symposium in Stuttgart, W. Germany, Sept. 1974.
3. Brown, D. C., *Application of Close Range Photogrammetry to Measurements of Structures in Orbit*, Geodetic Services Inc. (GSI) Technical Report No. 80-012, Vols. I and II, prepared under contract to Rockwell International, Space Systems Group, Dept. 379, Downey, CA, September 1980.
4. Brown, D. C., *STARS (Simultaneous Triangulation and Resection System) A Turnkey System for Close Range Photogrammetry*, Geodetic Services Inc. (GSI) Technical Report No. 82-007, March 10, 1982.
5. Fraser, C. S., *Photogrammetric Measurement of Microwave Antennas*, Geodetic Services Inc. (GSI) Technical Report No. 86-001, May 1986.
6. Chian, C. T., and Levy, R. "Load-Deflection Tests and Computer Analysis of a High-Precision Adhesive-Bonded Antenna Reflector Panel," *TDA Progress Report 42-82*, pp. 68-81, Jet Propulsion Laboratory, Pasadena, Calif., August 1985.

**Table 1. Activities for the PGM panel test**

Day No.	Description
1	Panels aligned on floor jigs, and targets placed.
2	2-man crew arrived on site. Photography of two panels. Developed and checked the films for four networks. Packed equipment and departed site (10-hr stay)
3	Film shipped by air.
4	Film arrived at GSI in Melbourne, Florida. Coordinates were read on the automated film comparator.
5	Verified the reference planes for the data. The computations were completed, the data plotted the same day.

**Table 2. Predicted PGM accuracy as given by Simulator output for large panel No. 9**

Number of Stations	Sigmas (rms), mm (inch)	Coordinate
4	0.028 (0.0011)	X
4	0.028 (0.0011)	Y
4	0.033 (0.0013)	Z

**Table 3. Actual PGM test accuracy**

Panel No.	Number of Stations	Sigma (rms), mm (inch)	Precision Ratio <sup>a</sup> , sigma/object diameter
3 (small)	8	0.013 (0.0005)	1/230,000
9 (large)	8	0.013 (0.0005)	1/270,000

<sup>a</sup>This is taken as 2.91 m (9.55 ft) for the small panel diagonal and 3.47 m (11.40 ft) for the large panel diagonal.

**Table 4. Sample results for small panel No. 3**

Point No.	Coordinates, inch		
	X	Y	Z
1	-37.1161	38.6390	0.1638
2	-31.3560	-8.8819	-0.5642
3	-27.1867	-42.4212	0.3118
101	-35.7950	-35.1000	0.0000 <sup>a</sup>
102	-34.6751	26.1338	-0.2728
108	-27.0827	-35.0917	0.0000 <sup>a</sup>
201	-29.2056	32.8568	-0.3791
1208	20.2674	-36.7120	-0.1152
1301	35.7950	35.1000	0.0000 <sup>a</sup>
1308	26.7389	-35.1347	-0.0024 <sup>b</sup>
1601	-40.8885	41.7420	-0.0902

<sup>a</sup>Points 101, 108 and 1301 make the reference plane.

<sup>b</sup>Point 1308 (not used in datum) shows a 0.0024 inch offset.

**Table 5. Sample results for large panel No. 9**

Point No.	Coordinates, inch		
	X	Y	Z
1	-42.6167	53.1027	0.11152
101	-41.5000	48.7352	0.0000 <sup>a</sup>
102	-41.4862	38.5145	-0.1795
110	-41.5000	-48.7352	0.0000 <sup>a</sup>
1701	-41.3086	-44.4043	0.0000 <sup>a</sup>
1710	31.2793	-52.5865	0.0078 <sup>b</sup>
2007	-9.9926	-49.8801	-0.3225

<sup>a</sup>Points 101, 110 and 1701 form the reference plane.

<sup>b</sup>Point 1710 (not used in datum) shows a 0.0078 inch offset.

**Table 6. Theoretical variation of PGM accuracy as a function number of stations**

No. of Stations, or Lines per Object	1-Sigma (rms), mm (inch)	Precision Ratio <sup>a</sup> sigma/object dia
8	0.013 (0.00050)	1/250,000 (actual)
4	0.018 (0.00071)	1/177,000
16	0.009 (0.00035)	1/350,000

<sup>a</sup>Based on an average panel diagonal of 3.2 m (10.4 ft).

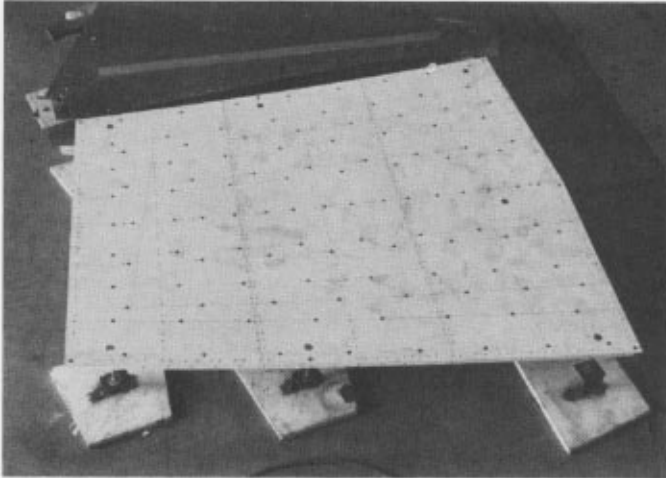


Fig. 1. Small panel No. 3 with PGM targets

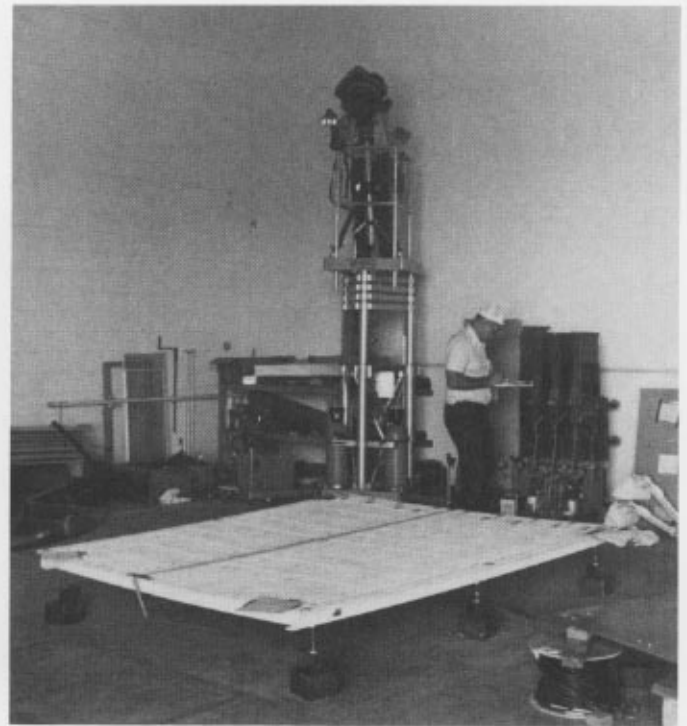


Fig. 3. Camera position relative to panel No. 9

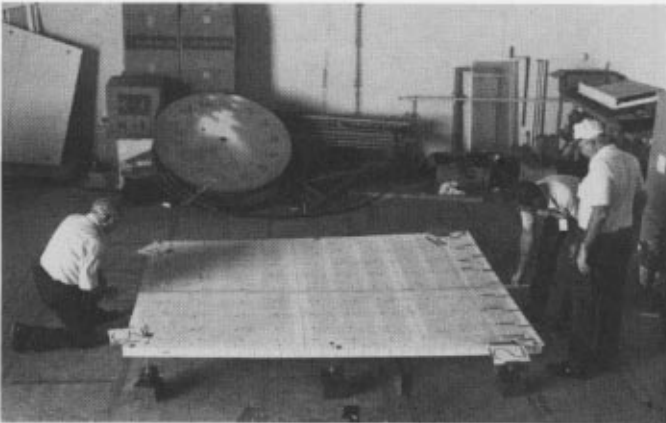


Fig. 2. Installation of scale tape on large panel No. 9



Fig. 4. Two panels ready for photography

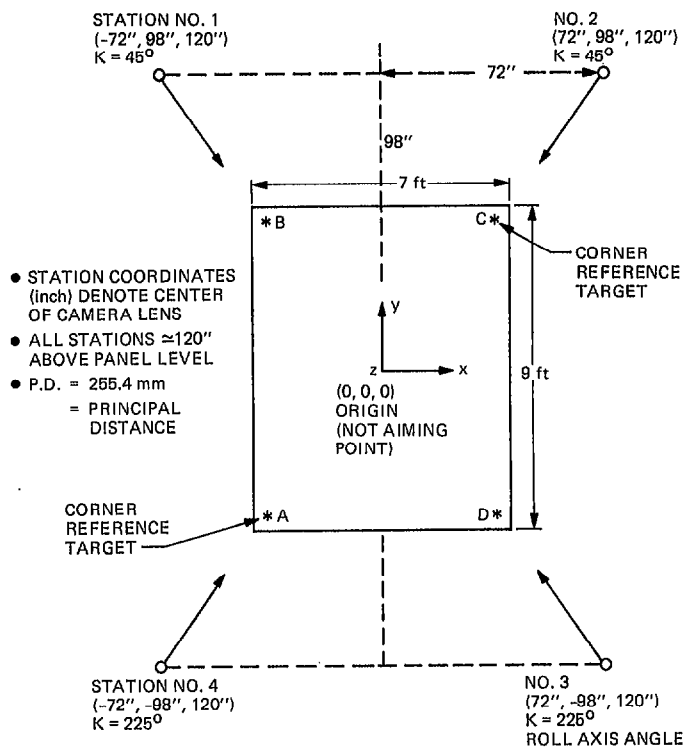


Fig. 5. Camera station locations relative to large panel No. 9

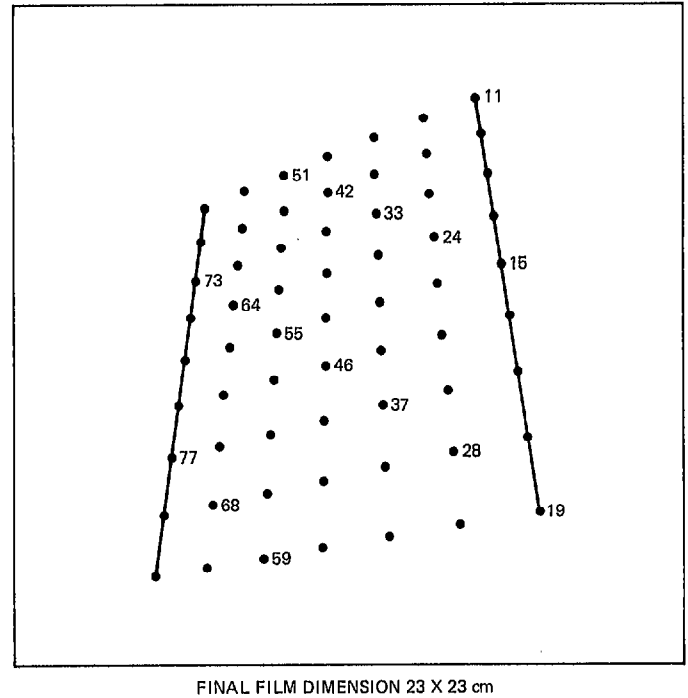


Fig. 6. Simulator output for camera station No. 1

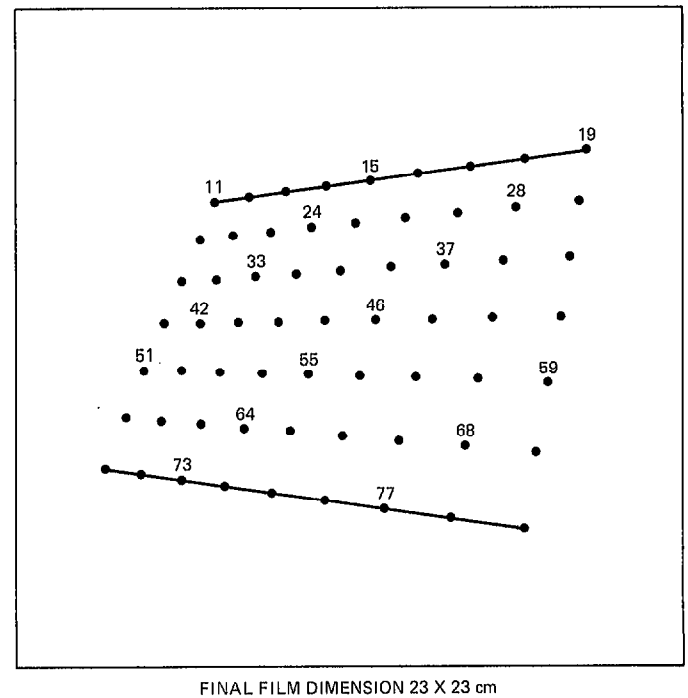
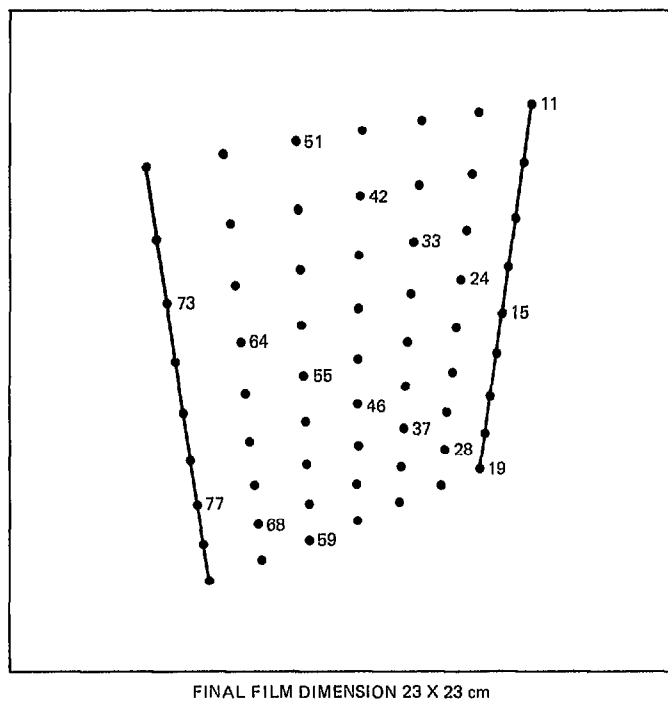


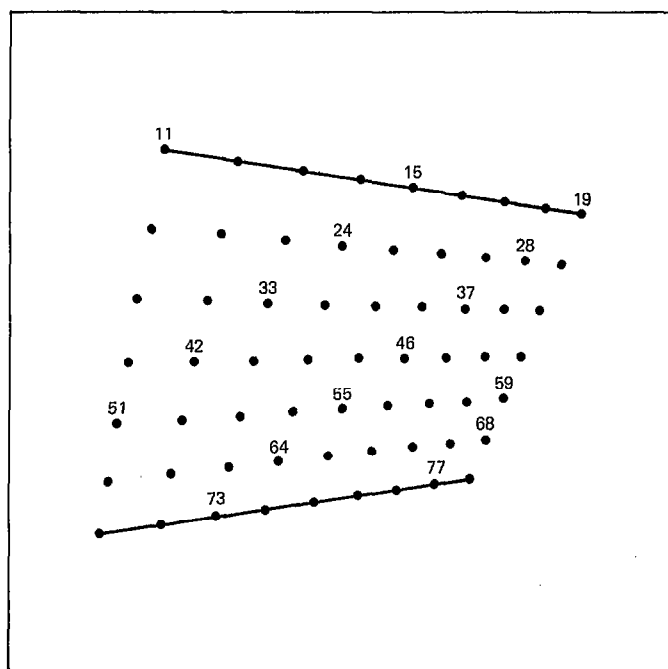
Fig. 7. Simulator output for camera station No. 2





FINAL FILM DIMENSION 23 X 23 cm

**Fig. 8. Simulator output for camera station No. 3**



FINAL FILM DIMENSION 23 X 23 cm

**Fig. 9. Simulator output for camera station No. 4**

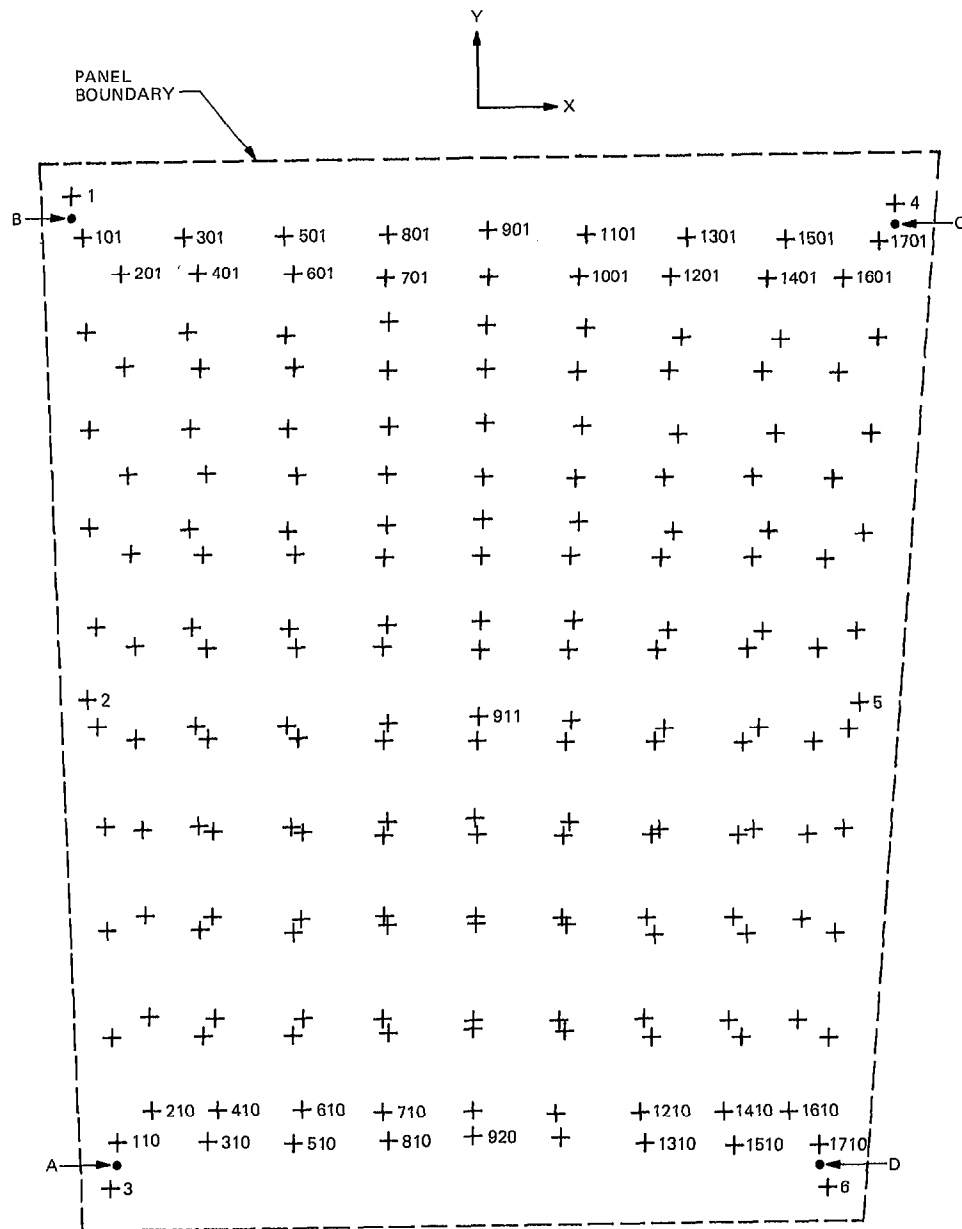


Fig. 10. Target distribution for large panel No. 9

## Appendix A

### Model for Best-Fit Parabola Computation to PGM Data

#### I. Model for Ideal Paraboloid

The basic equation of a paraboloid of revolution, as shown in Figure A-1, is:

$$x_p^2 + y_p^2 = 4fz_p$$

or

$$x_p^2 + y_p^2 + z_p^2 = 4fz_p + z_p^2 \quad (\text{A.1})$$

Let

$$\xi = \begin{bmatrix} x_p \\ y_p \\ z_p \end{bmatrix} \quad (\text{A.2})$$

hence,

$$[\xi]^T [\xi] = 4fz_p + z_p^2 \quad (\text{A.3})$$

The objective is to develop transformation equations between the measured  $(x, y, z)$  photogrammetric coordinates (with arbitrary origin and orientation) and best-fit paraboloid of revolution coordinates  $(x_p, y_p, z_p)$  with origin at the vertex. Transformation is achieved through a vertex translation to  $(x_0, y_0, z_0)$  and by two axial rotations  $(\alpha$  and  $\omega)$ .

$$\begin{bmatrix} x_p \\ y_p \\ z_p \end{bmatrix} = \begin{bmatrix} -\cos \alpha & \sin \alpha & 0 \\ -\sin \alpha \sin \omega & -\cos \alpha \sin \omega & \cos \omega \\ \sin \alpha \cos \omega & \cos \alpha \cos \omega & \sin \omega \end{bmatrix} \begin{bmatrix} x - x_0 \\ y - y_0 \\ z - z_0 \end{bmatrix} \quad (\text{A.4})$$

or

$$[\xi] = [R] [\eta]$$

Substitution of Equation (A.4) into (A.3) yields:

$$[\eta]^T [R]^T [R] [\eta] = 4fz_p + z_p^2$$

because  $R$  is unitary orthogonal

$$[R]^T [R] = [I]$$

hence,

$$\eta^T \eta = 4fR_3 \eta + (R_3 \eta)^2 \quad (\text{A.5})$$

where  $R_3$  is the third row of  $R$  given by:

$$R_3 = [D \ E \ F] = [\sin \alpha \cos \omega \quad \cos \alpha \cos \omega \quad \sin \alpha] \quad (\text{A.6})$$

Equation (A.5) can now be expanded into the form:

$$\begin{aligned} 0 &= (x - x_0)^2 + (y - y_0)^2 + (z - z_0)^2 \\ &\quad - 4f[D(x - x_0) + E(y - y_0) + F(z - z_0)] \\ &\quad - [D(x - x_0) + E(y - y_0) + F(z - z_0)]^2 \end{aligned} \quad (\text{A.7})$$

In computing a best-fit surface the six parameters  $x_0, y_0, z_0, \alpha, \omega$ , and  $f$  need to be computed. These parameters, along with the measured photogrammetric  $(x, y, z)$  coordinates make up the terms of Equation (A.7). Every point on the surface generates a separate equation.

Finding the best-fitting surface characteristics entails a solution of the parameters of Equation (A.7) via the method of least-squares through an iterative process with successive estimates of the 6 parameters. In linear form, a full observation equation set corresponding to Equation (A.7) can be written as follows:

$$[B] [r] + [A] [\delta] + [w] = 0 \quad (\text{A.8})$$

where

$[B]$  = sparse matrix of partial derivatives with respect to  $(x, y, z)$  coordinates computed at each point  $n$ . Dimensions  $(n \times 3n)$

$[r]$  = vector of coordinate residuals;  $r^T [r_{x1}, r_{y1}, r_{z1}, \dots, r_{xn}, r_{yn}, r_{zn}]$ . Dimensions  $(3n \times 1)$

$[A]$  = matrix of partial derivatives with respect to the parameters  $x_0, y_0, z_0, \alpha, \omega$  and  $f$ . Dimensions  $(n \times 6)$

and

$[\delta]$  = least-squares corrections to parameter estimates to yield most probable solution. Dimensions  $(6 \times 1)$

$$\delta^T = [\delta x_0, \delta y_0, \delta z_0, \delta \alpha, \delta \omega, \delta f]^T$$

and

$[w]$  = value of Eq. (A.7) using measured  $(x, y, z)$  coordinates and using estimates for parameter  $x_0, y_0, z_0, \alpha, \omega$ , and  $f$ .

where  $n$  is the number of photogrammetric points.

The solution to the overdetermined system, Equation (A.8), is given by:

$$[\delta] = -[A^T(BP^{-1}B^T)^{-1}A]^{-1}[A^T(BP^{-1}B^T)^{-1}w] \quad (A.9)$$

where  $P$  is the weight matrix corresponding to the variances of the  $x, y, z$  coordinates.

The accuracy estimates ( $\sigma$ , standard error value) for the parameters are obtained as:

$$C_6 = \begin{bmatrix} \sigma_{x_0}^2 & \cdot & \cdot & \cdot & \cdot & \cdot \\ \cdot & \sigma_{y_0}^2 & \cdot & \cdot & \cdot & \cdot \\ \cdot & \cdot & \sigma_{z_0}^2 & \cdot & \cdot & \cdot \\ \cdot & \cdot & \cdot & \sigma_{\alpha}^2 & \cdot & \cdot \\ \cdot & \cdot & \cdot & \cdot & \sigma_{\omega}^2 & \cdot \\ \cdot & \cdot & \cdot & \cdot & \cdot & \sigma_f^2 \end{bmatrix}$$

$$= \sigma_0^2 (A^T(BP^{-1}B^T)^{-1}A)^{-1} \quad (A.10)$$

where  $\sigma_0^2$  is the variance factor.

The solution for  $x_0, y_0, z_0, \alpha, \omega$  and  $f$  which is an iterative procedure minimizes the quadratic form  $r^T Pr$  where:

$$r^T Pr = \sum_{i=1}^n \left( \frac{r_{x_i}^2}{\sigma_{x_i}^2} + \frac{r_{y_i}^2}{\sigma_{y_i}^2} + \frac{r_{z_i}^2}{\sigma_{z_i}^2} \right) \rightarrow \text{minimum} \quad (A.11)$$

Here,  $\sigma_{x_i}^2, \sigma_{y_i}^2$ , and  $\sigma_{z_i}^2$  are coordinate standard errors.

Once the six parameters of the best-fit-parabola are computed, the corresponding point on parabola  $(x_p, y_p, z_p)$ , coordinates are computed from Equation (A.4). The  $z$ -departure is then defined as:

$$Dz = z_p^{(\text{measured})} - [(x_p^2 + y_p^2)/4f] \quad (A.12)$$

The RMS value for the surface is computed by:

$$\text{RMS of } Dz \text{ values} = [\sum (Dz^2)/n]^{1/2} \quad (A.13)$$

where " $n$ " is the number of photogrammetric points.

## II. Model for Quasi Paraboloid (e.g., Shaped Surfaces)

Initially,  $x_0, y_0, z_0, \alpha, \omega$ , and  $f$  are computed according to the above model. Because the surface is not a parabola, however, the  $z_p$  origin of the parabola coordinates is not strictly defined ( $f$  is also not applicable). Given a shape profile for the surface in the form of:

$$z'_p = f(r) \quad (A.14)$$

the  $z_p$  origin is defined such that

$$\sum_{i=1}^n (z_p - z'_{p_i}) = 0 \quad (A.15)$$

That is, the sum of all the final computed  $z$ -departure is zero. The computed offset to  $z_p$ , namely  $\delta z_p$ , is then applied to the parabola  $z_p$  coordinates such that Equation (A.15) is satisfied. The surface RMS value is then given as

$$\text{RMS of } Dz_p \text{ value} = \left\{ \sum_{i=1}^n \frac{[z_{p_i}^{(\text{final})} - z'_{p_i}]^2}{n} \right\}^{1/2} \quad (A.16)$$

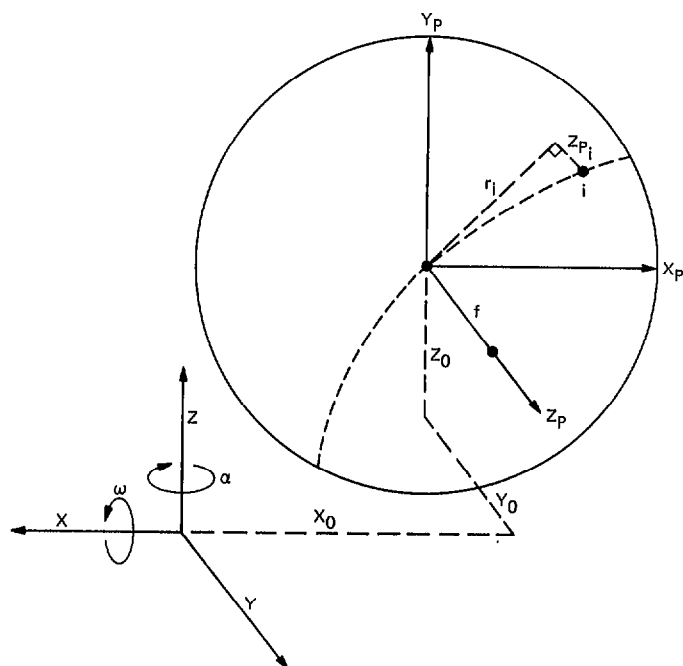


**Fig. A-1. Coordinates for best-fit paraboloid**